Journal of Solid State Chemistry **156,** 274–280 (2001)
doi:10.1006/jssc.2000.8952, available online at http://www.idealibrary.com on IDEAL®

Preparation and Characterization of VO_2 Nanopowders

Chenmou Zheng,[1] Xinmin Zhang, Jianhui Zhang, and Kairong Liao

School of Chemistry and Chemical Engineering, Zhongshan University, Guangzhou 510275, People's Republic of China
E-mail: daddy200@sina.com.

Received May 8, 2000; in revised from August 14, 2000; accepted September 5, 2000

VO_2 powders with sizes of < 30 nm were successfully synthesized by pyrolysis of the precursor, $[NH_4]_5[(VO)_6(CO_3)_4(OH)_9]\cdot 10H_2O$. The effects of various pyrolysis conditions on VO_2 stoichiometries and crystal states were investigated in detail. The results of IR measurements show that for the stoichiometric VO_2, from micro- to nanocrystals and to amorphous state, the absorptions shifted to lower wavenumbers, the numbers of bands decreased gradually, and the widths of the bands broadened. Moreover, the IR spectra of nanocrystals were obviously different from those of microcrystals and amorphism. In comparison with stoichiometric VO_2 crystals, the IR absorptions of oxygen-rich VO_2 crystals clearly were blue shift, and those of oxygen-deficient VO_2 crystals lightly red shift. The heats and temperatures of phase transition from $VO_{1.96}$ to $VO_{2.07}$ were determined. The results indicate that the phase transition temperature of $VO_{2.02}$ is 70.1°C and has the maximum phase transition heat. © 2001 Academic Press

Key Words: **nano material; vanadium dioxide; IR spectra; heat of phase transition.**

1. INTRODUCTION

Since Morin (1) first reported a semiconductor–metallic transition in VO_2 in 1959, VO_2 has been experimentally and theoretically studied by many material scientists. VO_2 exhibits a semiconductor-to-metal transition at about 68°C accompanied by a crystallographic transition from a low-temperature monoclinic form to a high-temperature tetragonal phase. This phase transition is associated with abrupt changes in optical and electrical properties; therefore, VO_2 has potential applications, for example, in preparing thermal and optical switches (2, 3). Although various technologies have been developed for producing VO_2 films (4, 5), few convenient ones have been found for making VO_2 powders. The typical method of preparing VO_2 powders is to heat a mixture of V_2O_3 (or V) and V_2O_5 corresponding to VO_2 composition in an evacuated silica tube at 700°C for 2 days (6), or to reduce V_2O_5 powder in a platinum crucible under an inert atmosphere at 1200–1350°C for 3 days (7, 8). These methods only obtained bulk VO_2 powders. Fine VO_2 powders have attracted much attention in recent years because they can decrease stress to rupture in the material at phase transition. Several methods of preparing fine VO_2 powders have been reported in the literature. Lawton and Theby, (9) synthesized VO_2 powders less than 1 μm by evaporative decomposition of solution, using dilute solution of vanadyl sulfate hydrate at $\geq$ 740°C in a mixed flow of hydrogen–nitrogen with a conventional spray-pyrolysis reactor, but the products resided sulfur about atomically 1%. Tsang and Manthiram (10) produced B phase VO_2 powders about 0.2 μm by reducing K_3VO_4 solution using KBH_4 as a reductant. Toshiyuki *et al.* (11) synthesized VO_2 powders about 10 nm by laser-induced vapor-phase reaction. However, the preparation of various stoichiometry VO_2 powders, which exert a tremendous influence on the material properties, has not been investigated in detail, and this is the key point for its preparation.

In this paper, we report a novel method for synthesizing VO_2 nanopowders with various stoichiometries and crystalline states by pyrolysis of the precursor, $[NH_4]_5[(VO)_6(CO_3)_4(OH)_9]\cdot 10H_2O$. The choise of this precursor is based on the following considerations: (1) it is easily synthesized (12); (2) VO_2 nonapowders are expected to be obtained easily due to the release of large amount of gases during pyrolysis; (3) the composition of pyrolysis products (powders) can be controlled more easily; and (4) the products will not contain any impurity.

2. EXPERIMENTAL

2.1. Precursor Preparation

The route of precursor preparation was reported in an earlier work of ours (12):

$$V_2O_5 + HCl + N_2H_4\cdot 2HCl \rightarrow VOCl_2 + NH_4HCO_3$$

$$\rightarrow (NH_4)_5[(VO)_6(CO_3)_4(OH)_9]\cdot 10H_2O.$$

[1] To whom correspondence should be addressed.

0022-4596/01 $35.00

The crystals obtained were laid aside to allow them to grow for about 1 h, followed by washing with a saturated NH_4HCO_3 solution until no Cl^- ion was detected. The crystals were washed again by alcohol, then pulverized to ≤ 2 μm with a supersonic pulverizer.

2.2. Precursor Pyrolysis

The precursor was spread in a 210-mm long, 27-mm-diameter quartz boat. The pyrolysis was performed in ϕ 35-mm silica tube. A flow of nitrogen (99.99%) or a mixed flow of nitrogen and air was introduced into the system for 15 min to replace the air in the tube, then the tube was heated to a desired temperature, which was maintained for a preset time.

2.3. Characterization Starting Material and Products

The purities of the starting material V_2O_5 and the product VO_2 were determined by inductively coupled plasma-atomic emission spectroscopy (ICP-AES). The impurity content of V_2O_5 (C.P.) was about 1000 at. ppm, with Cr, Sb, and Ga as the main sources of impurity, and that of VO_2 products was 60–400 at. ppm, showing that the materials used in this study were purified in a precursor synthesis process. The content of V^{3+} or V^{5+} ions in VO_2 products was determined volumetrically using ferroin as an indicator (13). The VO_2 samples were dissolved in a mixed solution of phosphoric–sulfuric acid under CO_2 atmosphere. The results of this method were in agreement with those of thermogravimetric analysis. The errors involved in this method were estimated to be within the range 0.001 through 0.002 in x of $VO_{2\pm x}$. The vanadium content of stoichiometric VO_2 was determined volumetrically, and the observed and calculated data were respectively 61.48 and 61.45%.

XRD experiments were carried out on a D/max-3A diffractometer. The feature micrographs were obtained using a JEM100-CX-II TEM, in which the samples were dispersed in a 731 DP supper-dispersing agent solution. The infrared spectra were recorded on a Nicolet 5DX FT-IR spectrometer, here the samples were laid in a desiccator with argon gas and pressed in to KBr pellets quickly. DSC experiments were performed using a NETZSCH DSC-204, from -30 to 120°C with a heating rate of 10°C min^{-1}; the powders used here were laid in a desiccator with argon gas and P_2O_5 to prevent them from being oxidized and adsorbing moisture.

3. RESULTS AND DISCUSSION

3.1. Effects of Pyrolysis Conditions on Composition of Products

The effects of various pyrolysis conditions on the composition of the VO_2 products are shown in Figs. 1–4. It can be seen from Fig. 1a that under the same pyrolysis conditions the oxidation numbers of the products decreased with increasing precursor sizes. Observations by microscope revealed that the greater the size of precursor, the greater the size of its product. It was found that the product particles with greater size were porous. This particle structure is favorable to the reduction of the product by the released ammonia from precursor. It should be noted that the precursor sizes were roughly estimated because the precursor particles with greater size were not homogeneous and exist in monoclinic form.In Fig. 1a the point corresponding to the precursor with 11 μm in size deviated from the curve. This may be related to the poor crystallinity of the precursor used, which was not laid aside to allow it to grow during

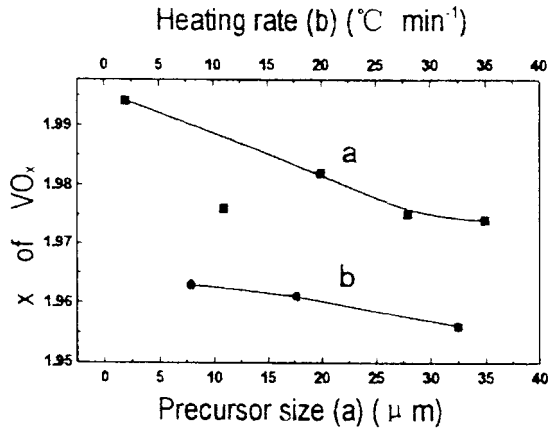

FIG. 1. Effects of precursor sizes and heating rates on product compositions: (a) precursor 3 g, N_2 3 L min^{-1}, air 8 ml min^{-1}, 600°C for 10 min, heating rate 26°C min^{-1}; (b) precursor 3 g, size ≤ 2 μm, N_2 3 L min^{-1}, air 0 ml min^{-1}, 450°C for 10 min.

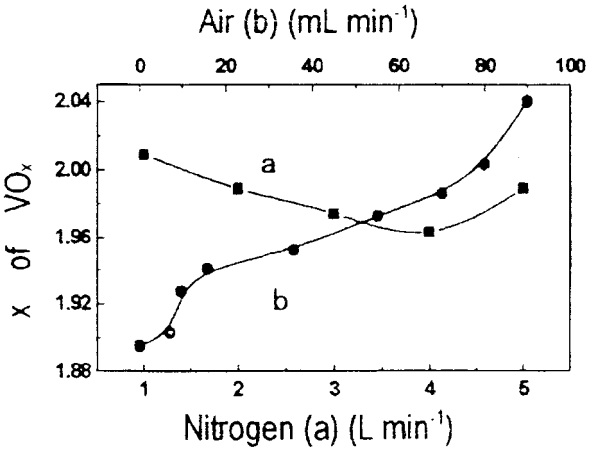

FIG. 2. Effects of nitrogen and air flow rates on product compositions: (a) precursor 5 g, air 4 ml min^{-1}, 450°C for 5 min; (b) precursor 5 g, N_2 4 L min^{-1}, 550°C for 5 min.

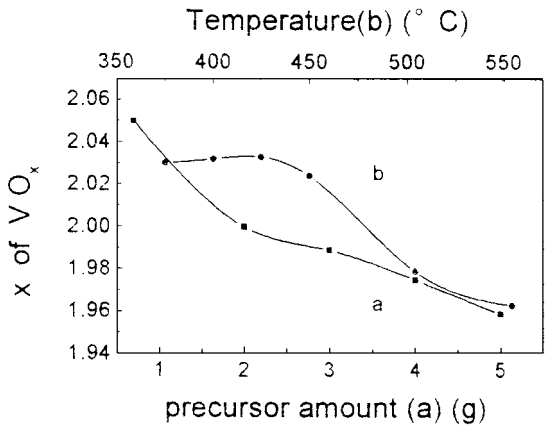

FIG. 3. Effects of precursor amounts and temperatures on product compositions: (a) N_2 3 L min^{-1}, air 7 ml min^{-1}, 550°C for 10 min; (b) precursor 3 g, N_2 3 L min^{-1}, air 10 ml min^{-1}, pyrolysis for 10 min.

preparation. Since the precursor crystals are in defect, the decomposition of the precursor may occur more quickly, and the ammonia concentration in the gas flow may increase at a certain moment; therefore, a deeply reduced product is produced. Figure 1b indicates that the oxidation numbers of the products lightly decreased with increasing heating rate. This phenomenon was similar to that mentioned above, due to the acceleration of the decomposition of the precursor at a higher heating rate. Considering the effects of the size of the precursor and the heating rate on the composition of the products, they were fixed at ≤ 2 μm and 26°C min^{-1} respectively, in the following researches.

Figure 2a shows the effects of nitrogen flow rate on the composition of the products. First, with increasing flow rate, the oxidation numbers of the powders decreased because reduction was more violent than oxidation during pyrolysis. However, as the flow rate increased up to 4 L min^{-1}, the oxidation number increased. The reason is that under higher flow rate the ammonia released during pyrolysis was driven away more quckly from the system so that the powder adsorption to ammonia was weakened. The effects of the air flow rate in nitrogen on the composition is shown in Fig. 2b. It indicates that the oxidation number increased with increasing air flow rate.

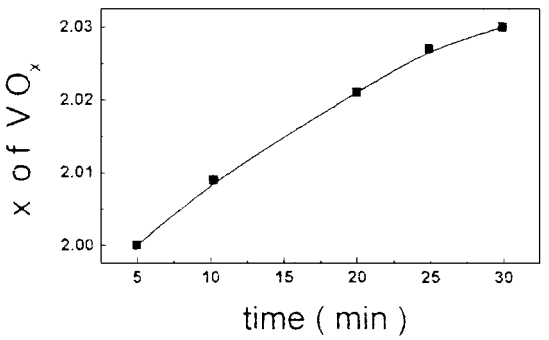

FIG. 4. Effect of pyrolysis times on product compositions: precursor 3 g, N_2 3 L min^{-1}, air 5 ml min^{-1}, at 450°C.

As displayed in Fig. 3a, the precursor amount has a great influence on the composition of the products, which may be attributed to the more amount of released ammonia in this case. Figure 3b shows the effects of temperature on the composition. Within the range 425 through 550°C, the oxidation number lowered as the temperature increased. According to the thermodynamic data calculated, the reduction power of ammonia on VO_2 is increased as temperature rises. However, it was found that as temperature went below 425°C, the composition did not vary wholly. This could be due to the presence of V(V) oxide in the products, which prevented VO_2 from being further oxidized. To observe the reduction of ammonia on the product, the following experiments were conducted. The precursor was pyrolyzed at 380°C under preset conditions and a $VO_{1.961}$ powder was obtained. Then, two other experiments were carried out as above, but was followed by cancelling the air flow in nitrogen and the temperature was elevated to 460 and 550°C, respectively, for 15 min. The compositions of the two powders obtained were $VO_{1.909}$ and $VO_{1.868}$. These results supported once again that the ammonia was not driven away from the system in time during pyrolysis but was strongly adsorbed by the powder, leading to the VO_2 being deeply reduced at high temperature. In fact, ammonia was detected in the product obtained at 550°C.

Figure 4 displays the effects of pyrolysis time on the composition. As the time was prolonged, the product was gradually oxidized and the oxidation numbers increased slowly.

It should be pointed out that the compositions of the products in the research have a good reproducibility and the experimental deviations are within the range of ± 0.004 in x of $VO_{2\pm x}$. Therefore, it can be concluded from the above results that the stoichiometry and various nonstoichiometries of VO_2 powders can be successfully synthesized by pyrolyzing the precursor under the selecting and controlling conditions.

3.2. *Crystallization of VO_2 Powder*

The crystallization process of VO_2 powder has been reported by some authors (14, 15) in the past, but the data were not wholly identical. The dependences of crystalline state on pyrolysis temperature and time determined by the XRD are shown in Fig. 5. The corresponding XRD patterns of the three various states in Fig. 5 are shown in Fig. 6. It can be seen from Fig. 5 that although the crystallization process was accelerated at higher temperature, pyrolyzing for a shorter time was unfavorable to the crystallization of VO_2 as the temperature was higher than 600°C owing to the

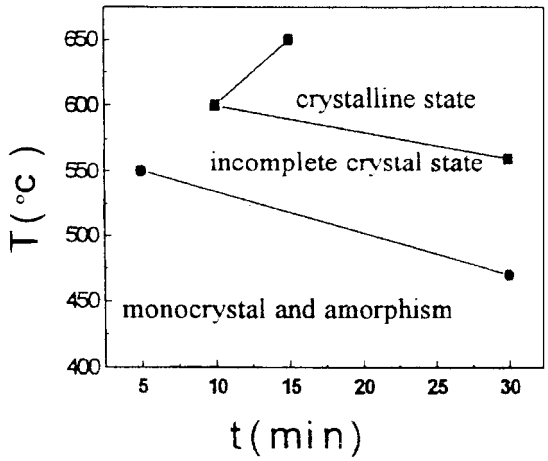

FIG. 5. Dependence of pyrolysis temperature and time on crystalline state of VO_2 powders.

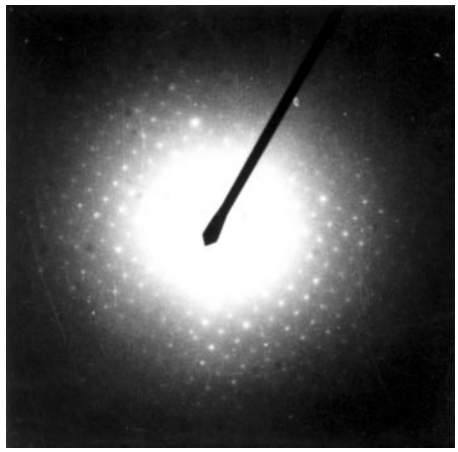

FIG. 7. Electron diffraction pattern from the sample obtained at 450°C for 20 min ($\times 10^5$).

violent reduction–oxidation in this case. Figure 6a shows that the powder obtained at 450°C for 20 min had very small peaks, indicating that it contained a few amount of crystals. In fact, as shown in Fig. 7 monocrystals have been found in the sample of Fig. 6a by electron diffraction. Therefore, the powder actually was a mixture of monocrystals and amorphism. The TEM micrographs of three various state powders are shown in Fig. 8. The sizes of amorphous state, incomplete crystal state, and crystalline state powders were about 10, 20, and 30 nm respectively. In addition, the particles of amorphism and incomplete crystals were looser and had rough surfaces, while the crystalline particle surfaces were smooth. These results demonstrate that the crystals growing slowly in the crystallization process formed larger particles. This was a result of the releasing of large amount of gases during pyrolysis of the precursor, which caused the particles to split and atomize strongly. Moreover, the powder adsorption to gases also inhibited the particles from growing. According to the results of seven crystalline samples calculated by the Scherrer equation, the powder sizes were 23.8–38.2 nm, which corresponded to those of TEM.

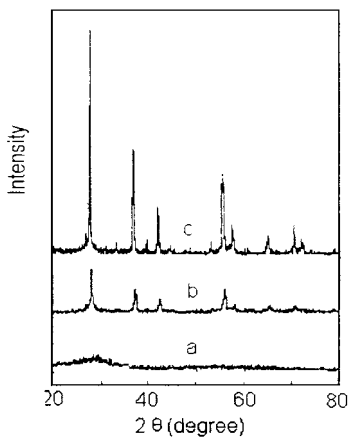

FIG. 6. Typical XRD patterns of various crystalline state VO_2 powders:(a) 450°C for 20 min, (b) 550°C for 20 min, (c) 600°C for 30 min

3.3. *Infraed Spectra of VO_2 Products*

The IR spectra of bulk crystal VO_2 has been studied (16–18) in recent years. Botto *et al.* (18) showed the IR spectra of a VO_2 sample obtained from temperature-programmed reduction. Figures 9a and 9b show respectively the IR spectra of VO_2 microcrystals about 5 μm in size reported by Botto and VO_2 nanocrystals about 30 nm in size obtained at 600°C for 20 min in our work. It can be found that the absorption at 995 cm^{-1} for the micromaterial shifted to 990 cm^{-1} for the nanomaterial. The absorptions at 714, 677, 660, 640, 620, and 599 cm^{-1} of the former were replaced by one broad, strong, and rather symmetric band of the latter. The absorptions at 521 and 508 cm^{-1} were degenerated into one symmetric band at 526 cm^{-1} . Finally, the shoulder band at 443 cm^{-1} became one separated band at 442 cm^{-1}. These results indicate that the IR behavior of nano-VO_2 is different from that of micro-VO_2 .

Figures 9c and 9d show respectively the IR spectra of the incomplete crystal VO_2 about 20 nm obtained at 500°C for 25 min and the amorphous state VO_2 with < 10 nm obtained at 380°C for 20 min. The absorption at 990 cm^{-1} of nanocrystals further shifted to 981 cm^{-1} for both materials. The absorptions at 917 and 901 cm^{-1} of the incomplete crystals and that at 880 cm^{-1} of the amorphous state were attributed to the vibration mode of V–OH because they had

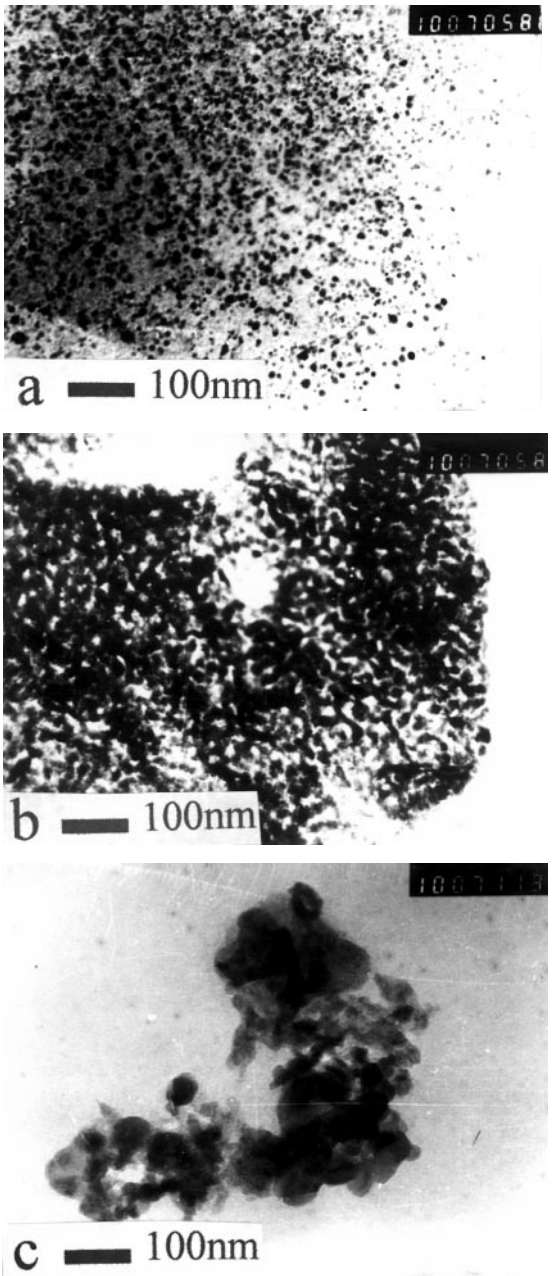

FIG. 8. TEM micrographs of the VO_2 powders: (a) amorphous state, 450°C for 10 min; (b) incomplete crystals, 550°C for 15 min; (c) crystals, 600°C for 30 min.

strong hygroscopicity. Moreover, the hygroscopic ability of the latter was greater far more than that of the former, so that the band at 880 cm^{-1} was very strong. The other bands also shifted to lower wavenumbers from crystals to incomplete crystals. However, the absorptions at 680 and 526 cm^{-1} for the crystals and those at 669 and 525 cm^{-1} for the incomplete crystals were replaced by one very broad and also symmetric absorption for the amorphous state. Also the bands close to 440 cm^{-1} were red shifted for the amorphous state.

The results above show that in the IR spectra from micro crystals to amorphous state, three main changes occurred; i.e., the wavenumbers of the absorptions lowered gradually, the band numbers decreased gradually, and the band widths broadened gradually. These phenomena were also observed in the IR spectra of microcrystals and amorphous state for some metal oxides (19). These characters can be used to distinguish various state VO_2 . Monoclinic VO_2 with chains of edge-shared VO_6 octahedra has various rigid V–O distances and uniformity in bond angles, which cause more IR absorptions as showed in Fig. 9a. The amorphous state has no unit cell and no correlated vibrations; therefore, its bands decrease. Since the V–O bond in amorphous state is not limited by crystal lattice, the V–O distance gets longer and the bond angles and the V–O distances are nonuniform, thus causing the wavenumbers to lower and the bands to broaden. Nanocrystals are in the middle state between microcrystals and amorphism and have numerous boundaries of crystals and a huge specific surface area; thus its IR spectra were obviously different from those of microcrystals. However, they exist in a crystalline state after all, so that their spectral characters were much different from those of amorphism.

Figures 9e and 9f show the IR spectra of the $VO_{1.97}$ about 30 nm and $VO_{2.03}$ with < 35 nm crystals obtained at 600°C for 20 min. Compared with those of stoichiometric VO_2 nanocrystals, the IR absorptions of $VO_{1.97}$ shifted to lower wavenumbers lightly, and those of $VO_{2.03}$ shifted to higher wavenumbers clearly. These characteristics were also favorable to distinguishing various stoichiometry VO_2 crystals . As the ionic radius is increased gradually from V(V) to V(III), the V–O bond length increases with the consequent softening of the vibration; thus appreciable shifts of V–O bands in the front region of the spectra toward smaller wavenumbers were observed from $VO_{2.03}$ to $VO_{1.97}$.

3.4. Transition Behavior of Various Stoichiometry VO_2

The effects of various stoichiometry VO_2 on the electrical resistivity and temperature at phase transition in monocrystals are different throughout the literature. For example, Kimizuka *et al.* (20) reported that from $VO_{2.00}$ to $VO_{2.07}$ the changes of resistivity were from 1.3×10 to 2×10^4 accompanied with the variances of transition temperatures from 63 to 71°C. However, Brückner *et al.* (21) observed that from $VO_{1.994}$ to $VO_{2.000}$ the changes of resistivity were from 6.3×10 to 1.3×10^4 with the variances from 58 to 69°C. Phase transition resistivity for polycrystalline VO_2 has not been reported so far, and the effects of various stoichiometry VO_2 in both monocrystals and polycrystals on phase transition heat also have not been reported. In this

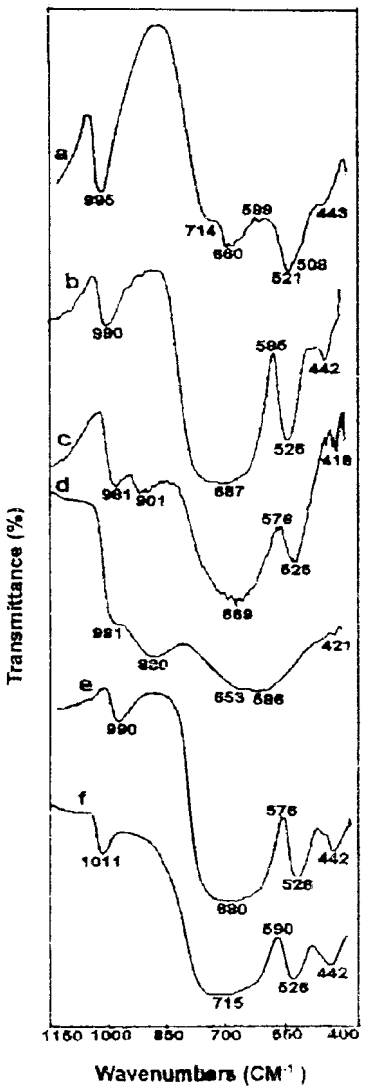

FIG. 9. IR spectra of various powders: (a) micro crystal VO_2, (b) nano crystal VO_2, (c) incomplete crystal VO_2, (d) amorphous state VO_2, (e) nano crystal $VO_{1.97}$, (f) nano crystal $VO_{2.03}$.

paper, the heats and the temperatures at transitions from $VO_{1.96}$ to $VO_{2.07}$ were measured, the results are listed in Table 1. The typical DSC scans of the products are shown in Fig. 10. The results indicate that the transition heats of the oxygen-deficient VO_2 were less than those of the oxygen-rich VO_2, and the $VO_{2.02}$ had the maximum transition heat.

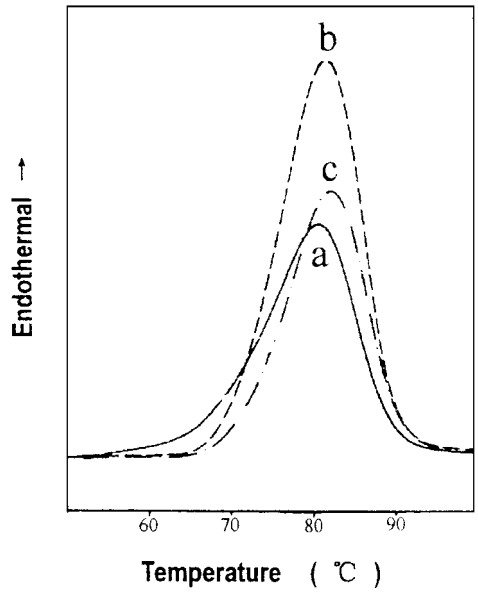

FIG. 10. DSC scans of VO_2 crystals: (a) — $VO_{1.98}$, (b) – – – $VO_{2.02}$, (c) –·–·– $VO_{2.05}$.

The transition temperatures were increased about 10°C from $VO_{1.96}$ to $VO_{2.07}$. Unfortunately, the VO_2 phase transition behavior has not been analyzed quantitatively so far.

4. CONCLUSION

VO_2 nanopowders with various stoichiometries and crystalline states were synthesized by pyrolyzing the precursor, $[NH_4]_5[(VO)_6(CO_3)_4(OH)_9]\cdot 10H_2O$, at low temperature under appropriate conditions. The IR spectra show that, from microcrystals to amorphism, the absorptions shift to lower wavenumbers with degenerating and broadening due to size and crystal effects. Moreover, from oxygen-rich to oxygen-deficient VO_2 crystals, the bands shift to lower wavenumbers due to the increasing V–O distance. DSC results indicate that the phase transition temperature of $VO_{2.02}$ is 70.1°C and possesses the maximum phase transition heat, which is different from those reported in the literature.

TABLE 1
Heats and Temperatures of Phase Transition

x in VO_x	1.96	1.98	2.00	2.01	2.02	2.03	2.04	2.05	2.07
ΔH (J/g)	24.17	37.92	45.64	49.12	56.75	52.53	46.36	37.77	34.03
T_t (°C)	60.7	68.0	68.8	68.7	70.1	69.6	69.7	70.9	69.0

ACKNOWLEDGMENT

This work was supported by the Natural Science Foundation (No.970168) of Guangdong Province of China.

REFERENCES

1. F. J. Morin, *Phys. Rev. Lett*. **3,** 34 (1959).
2. F. A. Chudnovskii, *Sov. Phys.* **20,** 999 (1976).
3. K. Eugeniusz, *Electron Technol.* **26,** 129 (1993).
4. C. D. E. Lakeman and D. A. Payne, *Mater. Chem. Phys.* **38,** 305 (1994).
5. C. Sella, M. Maaza, O. Nemraoui, J. Lafait, N. Renard, and Y. Sampeur, *Surf. Coat. Technol.* **98,** 1477 (1998).
6. Y. Bando, M. Kyoto, T. Takada, and S. Muranak, *J. Crystal Growth* **45,** 20 (1978).
7. N. Kimizuka, M. Isahii, I. Kawada, M. Saeeki, and M. Nakahira, *J. Solid State Chem.* **9,** 69 (1974).
8. J. B. Macchesney and H. J. Guggenheim, *J. Phys. Chem. Solids* **30,** 225 (1969).
9. S. A. Lawton and E. A. Theby, *J. Am. Ceram. Soc.* **78,** 104 (1995).
10. C. Tsang and A. Manthiram, *J. Electrochem. Soc.* **144,** 520 (1997).
11. O. Toshiyuki, I. Yasuhiro, and R. K. Kenkyu, *J. Photopolym. Sci. Technol.* **10,** 211 (1997).
12. T. C. W. Mak, P. Li, C. Zheng, and K. Huang, *J. Chem. Chem. Commun.* 1597 (1986).
13. G. G. Rao and P. K. Rao, *Talanta* **13,** 1335 (1966).
14. F. Theobald, R. Cabala, and J. Bernard, *J. Solid State Chem.* **17,** 431 (1976).
15. J. R. Dahn, T. V. Buuren, and U. Vonsachen, U. S. Patent 4,965,150 (1990).
16. A. Heinrich, E. I. Terukov, W. Reichelt, H. Wagner, and H. Oppermanm, *Phys. Stat. Sol.* (*a*) **72,** K61 (1982).
17. T. A. Hewston, and M. P. Nadler, *J. Sol. Stat. Chem.* **71,** 278 (1987).
18. I. L. Botto, M. B. Vassallo, E. J. Baran, and G. Minelli, *Mater. Chem. Phys.* **50,** 267 (1997).
19. W. E. Steger, H. Landmesser, U. Boettcher, and E. Schubert, *J. Mol. Struct.* **217,** 341 (1990).
20. N. Kimizuk, M. Ishii, I. Kawada, M. Saeki, and M. Nakahira, *J. Solid State Chem.* **9,** 69 (1974).
21. W. Brückner, W. Moldenhauer, H. Wich, E. Wolf, H. Oppermann, U. Gerlach, and W. Reichelt, *Phys. Stat. Sol.* (a) **29,** 63 (1975).